Earth Planets Space, **54**, 917–926, 2002

Shear instabilities in the dust layer of the solar nebula III. Effects of the Coriolis force

Naoki Ishitsu[1] and Minoru Sekiya[2]

[1]*Department of Earth and Planetary Sciences, Graduate School of Sciences, 33 Kyushu University, Hakozaki, Fukuoka 812-8581, Japan*
[2]*Department of Earth and Planetary Sciences, Faculty of Sciences, 33 Kyushu University, Hakozaki, Fukuoka 812-8581, Japan*

(Received May 24, 2002; Revised September 2, 2002; Accepted September 6, 2002)

In previous our papers (Sekiya and Ishitsu, 2000 and 2001), hydrodynamic stability of the dust layer in the solar nebula is investigated. However, these papers neglected the rotational effects, that is, the Coriolis and tidal forces. These forces may stabilize the shear instability of the dust layer. In this paper, the linear stability analysis with the Coriolis and without tidal force is done in order to elucidate the effects of the Coriolis force. Our results indicate that the growth rates of the instabilities are similar between the cases with and without the Coriolis force. However, we found a new type of instability which resembles the Lindblad resonance. This instability only emerges if the growth rate is similar to or smaller than the Keplerian angular frequency. The energy source of the instability is different from that of the shear instability.

1. Introduction

In the past, planetesimals were considered to be formed by the gravitational instability in the dust layer (Safronov, 1969; Goldreich and Ward, 1973; Coradini *et al.*, 1981; Sekiya, 1983). However, the occurrence of gravitational instability is suspect because of the following reason. Imagine a fluid element in the solar nebula consists of gas and dust aggregates. Assume the aggregates are small and/or fluffy enough to move approximately with the same velocity with the gas due to the drag force. Then the revolution velocity of the fluid element is determined by the balance of the gravity of the central star, the centrifugal force, and the pressure gradient. The former two act on both the gas and dust aggregates. On the other hand, the latter acts only on the gas. Thus, the revolution velocity depends on the dust to gas mass ratio and, hence, vertical shear arises in the dust layer as dust aggregates settle toward the midplane. Indeed, the balance of these forces are written

$$-\frac{GM_*}{r^2}+\frac{(v+v_K)^2}{r}-\frac{1}{\rho}\frac{\partial P_g}{\partial r}=0, \qquad (1)$$

where G is the gravitational constant, M_* is the mass of the central star, $v_K = (GM_*/r)^{1/2}$ is the circular Kepler velocity, v is the gas velocity relative to v_K, r is the distance from the rotation axis, P_g is the gas pressure, and ρ is the total fluid density defined by

$$\rho = \rho_g + \rho_d, \qquad (2)$$

where ρ_g is the gas density and ρ_d is the dust density. Solving Eq. (1) by neglecting v^2, we have

$$v = -\frac{\rho_g}{\rho}\eta v_K, \qquad (3)$$

where η is a non-dimensional parameter which represents the effect of the radial pressure gradient:

$$\eta = -\frac{r}{2\rho_g v_K^2}\frac{\partial P_g}{\partial r}, \qquad (4)$$

(Adachi *et al.*, 1976; Nakagawa *et al.*, 1986; Sekiya, 1998). The ratio ρ_g/ρ depends on the vertical level owing to dust settling; hence, the revolution velocity v has vertical shear. This vertical shear may cause the shear instability, which may develop turbulence in the dust layer. The turbulence stirs up the dust from the midplane. Thus, the density at the midplane cannot exceed the critical density of the gravitational instability (Weidenschilling, 1980). Subsequently, many authors have investigated this issue (Weidenschilling, 1984; Cuzzi *et al.*, 1993; Weidenschilling and Cuzzi, 1993; Champney *et al.*, 1995; Sekiya, 1998; Dobrovolskis *et al.*, 1999). They also concluded that the turbulence prevents the dust from settling and that the formation model of planetesimals through the gravitational fragmentation of the dust layer is denied. Planetesimals are considered to have been formed by continuous sticking of dust aggregates.

However, the shear instability in the dust layer is not understood enough. In order to elucidate the nature of the shear-induced instability, we have performed linear calculations of the perturbation equations of the fluid mechanics in previous papers (Sekiya and Ishitsu, 2000 and 2001, hereafter referred to as Papers I and II, respectively) under the following assumptions: (1) The self-gravity is neglected. (2) A mixture of gas and dust is treated as one fluid, which is a good approximation in the case where dust aggregate sizes are small ($\lesssim$1 cm). (3) The solar tidal force, which is the sum of the radial component of the solar gravity and the centrifugal force, is neglected; thus the radial shear $\partial v/\partial r$ is not incorporated in the unperturbed state, and only z-component of the solar gravity is taken into account, where z is the coordinate perpendicular to the midplane of the solar nebula

($z = 0$ on the midplane). (4) The effects of the Coriolis force are neglected. (5) The effects of the radial density and pressure gradients of the unperturbed state are only incorporated in the unperturbed rotation velocity distribution $v_0(z)$. (6) Local Cartesian coordinates (x, y, z) are used and we neglect the curvature of a circle with constant values of r and z.

In Paper I, we further assumed for simplicity that the unperturbed densities had constant Richardson number density distributions. The results showed: (A) The flow is stable for the Richardson number $J \gtrsim 0.22$. (B) The growth time of the shear instability is much longer than the Kepler period, as long as the Richardson number $J \gtrsim 0.1$. On the other hand, the Coriolis and the tidal forces would affect the flow in time scale on the order of the Kepler period. Thus the neglect of these forces is not good for the constant Richardson number density distribution with $J \gtrsim 0.1$.

In Paper II, the linear stability analysis like Paper I was performed, but the hybrid density distribution was used:

$$\rho_{d0}(z) = \begin{cases} \rho_{d0}(0) \ \text{ for } |z| \le z_d - 2h_d, \\ \rho_{d0}(0)\{1 - \sin[\pi(z - z_d + h_d)/2h_d]\}/2 \\ \qquad \text{for } z_d - 2h_d < |z| < z_d, \\ 0 \ \text{ for } z_d \le |z|, \end{cases} \tag{5}$$

where $\rho_{d0}(0)$ is the dust density on the midplane, z_d is the half-thickness of the dust layer, and h_d is the half-thickness of the transition zones, where the dust density varies from $\rho_{d0}(0)$ to 0 sinusoidally. Here the half-thickness of the dust layer is given by

$$z_d = \frac{\Sigma_d}{2\rho_{d0}(0)} + h_d, \tag{6}$$

where we used Hayashi's solar nebula model (Hayashi, 1981; Hayashi *et al.*, 1985) at 1 AU as the dust surface density. The dust particles which are distributed uniformly at first stick together to form dust aggregates. In a laminar disk, the settling velocity v_{dz} of dust aggregate is given by

$$v_{dz} = -\tau_f \Omega_K^2 z, \tag{7}$$

which is τ_f is the frictional time of the dust aggregate. Thus, dust aggregates grow faster in regions with larger $|z|$, since the principal relative velocity of dust aggregates is induced by difference of settling velocities of dust aggregates with different frictional times (Weidenschilling, 1980; Nakagawa *et al.*, 1981). As dust aggregates grow, their settling velocities increase if the dust aggregates are compact. Thus, dust aggregates accumulate in a certain region with an intermediate value of $|z|$ (see 1000 yrs and 1300 yrs density distribution in figure 2 of Nakagawa *et al.* (1981)). This state is unstable for the Rayleigh-Taylor instability, and the dust density distribution is considered to be adjusted as to be constant in the dust layer (Watanabe and Yamada, 2000). According to results, if $\rho_d(0)/\rho_g \sim 1$, the growth rate of the instability is on the order of the Keplerian angular frequency. On the other hand, if $\rho_d(0)/\rho_g \gg 1$, the growth rate is much larger than the Keplerian angular frequency. Thus, we have expected that the Coriolis and tidal forces might not have an important effect as long as $\rho_d(0)/\rho_g \gg 1$.

In this paper, we remove assumption (4) above, that is, we take the effect of the Coriolis force into account. The hybrid dust density distributions of Paper II is adopted as the unperturbed dust density distributions. In Section 2, the basic equations for the linear analysis are derived. In Section 3, calculated results are given. In Section 4, the energy source of the instability is discussed. In Section 5, conclusions are written.

2. Formulation

We assume that dust aggregates are small and/or fluffy enough to couple well with the gas. Further, the half thickness of the dust layer is much smaller than the scale height of the disk gas and the gas density is nearly constant. Thus, the dust-gas mixture is treated as incompressible one-fluid. Hydrodynamic equations for dust-gas mixture in the local Cartesian co-ordinate system rotating with the local Kepler angular velocity Ω_K are given omitting the tidal force, by

$$\frac{\partial u}{\partial x} + \frac{\partial v}{\partial y} + \frac{\partial w}{\partial z} = 0, \tag{8}$$

$$\frac{\partial \rho}{\partial t} + u\frac{\partial \rho}{\partial x} + v\frac{\partial \rho}{\partial y} + w\frac{\partial \rho}{\partial z} = 0, \tag{9}$$

$$\frac{\partial u}{\partial t} + u\frac{\partial u}{\partial x} + v\frac{\partial u}{\partial y} + w\frac{\partial u}{\partial z} = -\frac{1}{\rho}\frac{\partial P}{\partial x} + 2C\Omega_K v, \tag{10}$$

$$\frac{\partial v}{\partial t} + u\frac{\partial v}{\partial x} + v\frac{\partial v}{\partial y} + w\frac{\partial v}{\partial z} = -\frac{1}{\rho}\frac{\partial P}{\partial y} - 2C\Omega_K u, \tag{11}$$

$$\frac{\partial w}{\partial t} + u\frac{\partial w}{\partial x} + v\frac{\partial w}{\partial y} + w\frac{\partial w}{\partial z} = -\frac{1}{\rho}\frac{\partial P}{\partial z} - \Omega_K^2 z, \tag{12}$$

where x and y represent the radial and azimuthal coordinates, and (u, v, w) are the (x, y, z) components of the velocity, and P is the pressure. Parameter C in Eqs. (10) and (11) is equal to unity in the real Keplerian disk. We calculated cases where $0 \le C \le 1$ in order to elucidate the effects of the Coriolis force.

In order to carry out linear calculation, we assume that the unperturbed state is steady and uniform in x and y directions:

$$\frac{\partial}{\partial t} = \frac{\partial}{\partial x} = \frac{\partial}{\partial y} = 0. \tag{13}$$

We also assume the unperturbed velocity has only azimuthal component (y-direction):

$$u_0 = w_0 = 0. \tag{14}$$

From Eqs. (10) and (12), we have

$$\frac{1}{\rho_0}\frac{\partial P_0}{\partial x} = 2C\Omega_K v_0, \tag{15}$$

and

$$\frac{1}{\rho_0}\frac{\partial P_0}{\partial z} = -\Omega_K^2 z, \tag{16}$$

respectively, where unperturbed density is defined by

$$\rho_0(z) = \rho_g + \rho_{d0}(z). \tag{17}$$

The unperturbed azimuthal velocity is calculated from a given dust density distribution ρ_{d0} and a given value of η by using Eq. (3):

$$v_0 = -\frac{\rho_g}{\rho_0}\eta v_K. \tag{18}$$

The radial pressure gradient $\partial P_0/\partial x$ in our model is then given by Eq. (15). Note that the value of $\partial P_0/\partial x$ is not equal to the value of $\partial P_g/\partial r$ in Eqs. (1) and (4) for $C \neq 1$. We solve the case $C < 1$ in order to elucidate the effect of the Coriolis force. Only the case with $C = 1$ is realistic, and then $\partial P_0/\partial x = \partial P_g/\partial r$.

Linearizing Eqs. (8)–(12) and using Eqs. (15) and (16), we have

$$\frac{\partial u_1}{\partial x} + \frac{\partial v_1}{\partial y} + \frac{\partial w_1}{\partial z} = 0, \tag{19}$$

$$\frac{\partial \rho_1}{\partial t} + v_0\frac{\partial \rho_1}{\partial y} + \frac{d\rho_0}{dz}w_1 = 0, \tag{20}$$

$$\frac{\partial u_1}{\partial t} + v_0\frac{\partial u_1}{\partial y} = -\frac{1}{\rho_0}\frac{\partial P_1}{\partial x} + 2C\Omega_K\frac{v_0}{\rho_0}\rho_1 + 2C\Omega_K v_1, \tag{21}$$

$$\frac{\partial v_1}{\partial t} + v_0\frac{\partial v_1}{\partial y} + \frac{dv_0}{dz}w_1 = -\frac{1}{\rho_0}\frac{\partial P_1}{\partial y} - 2C\Omega_K u_1, \tag{22}$$

$$\frac{\partial w_1}{\partial t} + v_0\frac{\partial w_1}{\partial y} = -\frac{1}{\rho_0}\frac{\partial P_1}{\partial z} - \frac{\Omega_K^2 z}{\rho_0}\rho_1. \tag{23}$$

We assume η, Ω_K, v_K, ρ_g and $\partial P_0/\partial x$ have constant values in the regime of the local approximation.

Here linear stability analysis is carried out in terms of same method as Paper I, II. We assume that perturbed quantities have the form as

$$f_1(x, y, z, t) = \hat{f}_1(z)\exp[i(k_x x + k_y y - \omega t)]. \tag{24}$$

If ω_I (the imaginary part of ω) is positive, the mode is unstable, and the growth rate is given by ω_I. Equations (19)–(23) is rewritten (We omit ˆ in the following equations)

$$ik_x u_1 + ik_y v_1 + \frac{dw_1}{dz} = 0, \tag{25}$$

$$-i\bar{\omega}\rho_1 + \frac{d\rho_0}{dz}w_1 = 0, \tag{26}$$

$$-i\bar{\omega}u_1 = -ik_x\frac{1}{\rho_0}P_1 + 2C\Omega_K\frac{v_0}{\rho_0}\rho_1 + 2C\Omega_K v_1, \tag{27}$$

$$-i\bar{\omega}v_1 = -ik_y\frac{1}{\rho_0}P_1 - \frac{dv_0}{dz}w_1 - 2C\Omega_K u_1, \tag{28}$$

$$-i\bar{\omega}w_1 = -\frac{1}{\rho_0}\frac{dP_1}{dz} - \frac{\Omega_K^2 z}{\rho_0}\rho_1, \tag{29}$$

where

$$\bar{\omega} = \omega - k_y v_0(z). \tag{30}$$

From Eq. (26), we have

$$\rho_1 = \frac{1}{i\bar{\omega}}\frac{d\rho_0}{dz}w_1. \tag{31}$$

From Eqs. (27), (28), and (31), we have

$$u_1 = \left[(k_x\bar{\omega} + 2iCk_y\Omega_K)\frac{P_1}{\rho_0} + 2C\Omega_K\left(\frac{v_0}{\rho_0}\frac{d\rho_0}{dz} + \frac{dv_0}{dz}\right)w_1\right]\left(\bar{\omega}^2 - 4C^2\Omega_K^2\right)^{-1}, \tag{32}$$

and

$$v_1 = \left[(k_y\bar{\omega} - 2iCk_x\Omega_K)\frac{P_1}{\rho_0} + \left(-i\bar{\omega}\frac{dv_0}{dz} + \frac{4C^2\Omega_K^2}{i\bar{\omega}}\frac{v_0}{\rho_0}\frac{d\rho_0}{dz}\right)w_1\right]\cdot\left(\bar{\omega}^2 - 4C^2\Omega_K^2\right)^{-1}. \tag{33}$$

Substituting Eqs. (32) and (33) into Eq. (25), we have

$$P_1 = -\frac{i\rho_0}{k^2\bar{\omega}}\left\{(\bar{\omega}^2 - 4C^2\Omega_K^2)\frac{dw_1}{dz} + \left[2iCk_x\Omega_K\left(\frac{v_0}{\rho_0}\frac{d\rho_0}{dz} + \frac{dv_0}{dz}\right) + k_y\left(\bar{\omega}\frac{dv_0}{dz} + \frac{4C^2\Omega_K^2}{\bar{\omega}}\frac{v_0}{\rho_0}\frac{d\rho_0}{dz}\right)\right]w_1\right\}. \tag{34}$$

Substituting Eqs. (31) and (34) into (29), we get

$$\frac{d^2w_1}{dz^2} + F\frac{dw_1}{dz} + Gw_1 = 0, \tag{35}$$

where

$$F = \frac{1}{\rho_0}\frac{d\rho_0}{dz} + \frac{k_y}{\bar{\omega}}\frac{dv_0}{dz} + \frac{1}{\bar{\omega}^2 - 4C^2\Omega_K^2}\left[2iCk_x\Omega_K\left(\frac{v_0}{\rho_0}\frac{d\rho_0}{dz} + \frac{dv_0}{dz}\right) - k_y\left(\bar{\omega}\frac{dv_0}{dz} - \frac{4C^2\Omega_K^2 v_0}{\bar{\omega}\rho_0}\frac{d\rho_0}{dz}\right)\right], \tag{36}$$

$$\begin{aligned} G = \frac{1}{\bar{\omega}^2 - 4C^2\Omega_K^2}\Bigg\{&-k^2\bar{\omega}^2 + 2iCk_x\Omega_K\left(\frac{1}{\rho_0}\frac{d^2\rho_0}{dz^2}v_0 + \frac{2}{\rho_0}\frac{d\rho_0}{dz}\frac{dv_0}{dz} + \frac{d^2v_0}{dz^2}\right) \\ &+ k_y\left[\bar{\omega}\left(\frac{1}{\rho_0}\frac{d\rho_0}{dz}\frac{dv_0}{dz} + \frac{d^2v_0}{dz^2}\right) - k_y\left(\frac{dv_0}{dz}\right)^2 + \frac{4C^2\Omega_K^2}{\bar{\omega}\rho_0}\left(v_0\frac{d^2\rho_0}{dz^2} + \frac{\omega}{\bar{\omega}}\frac{dv_0}{dz}\frac{d\rho_0}{dz}\right)\right] \\ &+ \frac{k_y}{\bar{\omega}}\frac{dv_0}{dz}\left[2iCk_x\Omega_K\left(\frac{v_0}{\rho_0}\frac{d\rho_0}{dz} + \frac{dv_0}{dz}\right) + k_y\left(\bar{\omega}\frac{dv_0}{dz} + \frac{4C^2\Omega_K^2}{\bar{\omega}}\frac{v_0}{\rho_0}\frac{d\rho_0}{dz}\right)\right] \\ &- k^2\frac{1}{\rho_0}\frac{d\rho_0}{dz}\Omega_K^2 z\Bigg\}, \end{aligned} \tag{37}$$

where

$$k^2 = k_x^2 + k_y^2.$$

Only odd solutions for w_1 are considered like Papers I and II since even ones are always stable according to our calculations. Thus, the boundary conditions are

$$w_1 = 0 \text{ at } z = 0. \tag{38}$$

Outside the dust layer, from Eqs. (35) to (37), we have

$$\frac{d^2 w_1}{dz^2} - K^2 w_1 = 0, \tag{39}$$

where

$$K^2 = \frac{k^2 \bar{\omega}^2}{\bar{\omega}^2 - 4C^2\Omega_K^2}. \tag{40}$$

We select a root K whose real part is positive. Then the outer boundary condition, i.e., $w_1 \to 0$ for $z \to \infty$, is satisfied by the solution,

$$w_1 \propto \exp(-Kz). \tag{41}$$

From Eq. (41), we have

$$\frac{dw_1}{dz} + Kw_1 = 0 \text{ for } z > z_d. \tag{42}$$

From Eqs. (34) and (42), we get

$$P_1 = -\frac{i\rho_g(\bar{\omega}^2 - 4C\Omega_K^2)}{k^2\bar{\omega}}\frac{dw_1}{dz} = \frac{i\rho_g(\bar{\omega}^2 - 4C\Omega_K^2)K}{k^2\bar{\omega}} w_1. \tag{43}$$

At the boundary between the dust and the gas layers, P_1 and w_1 must be continuous. Thus Eqs. (34) and (43) read

$$\frac{dw_1}{dz} + \left\{K + \frac{1}{\bar{\omega}^2 - 4C^2\Omega_K^2}\left[2iCk_x\Omega_K\left(\frac{v_0}{\rho_0}\frac{d\rho_0}{dz} + \frac{dv_0}{dz}\right) + k_y\left(\bar{\omega}\frac{dv_0}{dz} + \frac{4C^2\Omega_k^2}{\bar{\omega}}\frac{v_0}{\rho_0}\frac{d\rho_0}{dz}\right)\right]\right\} w_1 = 0 \text{ at } z = z_d. \tag{44}$$

3. Results

The effects of the Coriolis force are examined by varying the value of parameter C from 0 to 1. The growth rate of the instability is on the order of Ω_K when the system does not rotate, i.e. $C = 0$ (see Paper II). We expected the effect of the Coriolis force was significant when the growth rate of the instability was small. Figure 1 shows the growth rate of the instability with the most unstable wave number (hereafter called "the peak growth rate") as a function of C with $\rho_{d0}(0)/\rho_g = 1$, $k_x = 0$ and $h_d/z_d = 0.5$. As the value of C approaches 1, the peak growth rate decreases some extent but is rather insensitive to the parameter C, contrary to our expectation. Figure 2 displays the growth rate as a function of the azimuthal wave number for $C = 1$ and 0, with $k_x = 0$, $\rho_{d0}(0)/\rho_g = 1$ and $h_d/z_d = 0.5$. As seen from Figs. 2, the dependency of the growth rate on wave number is different for a different value of C. When $C = 0$, the growth rate have a peak at $\log(k_y^2\eta^2r^2) = 1.72$ and $k_x = 0$. As C increases, the peak wave number increases. For $C = 1$ the slope of the curve in Fig. 2 changes abruptly at $\log(k_y^2\eta^2r^2) = 1.8$ and the eigenvalue with $\omega_I > 0$ does not exist for $\log(k_y^2\eta^2r^2) > 2.2$.

In the case of $C = 0$, ω_I approaches zero gradually as k_x increases (see Fig. 3). On the other hand, in the case of $C = 1$, the growth rate ω_I has a finite positive value for $k_x < k_{xc}$, and $\omega_I = 0$ for $k_x > k_{xc}$, where k_{xc} is the critical radial wave number, and the position of the peak at fixed $\log(k_y^2\eta^2r^2)$ departs from $k_x = 0$, as seen in Fig. 4. In any rate, as the wave number k_x increases, the instability is stabilized. This is very important for the stability in the case including the effect of the tidal force, which will be written in our subsequent paper.

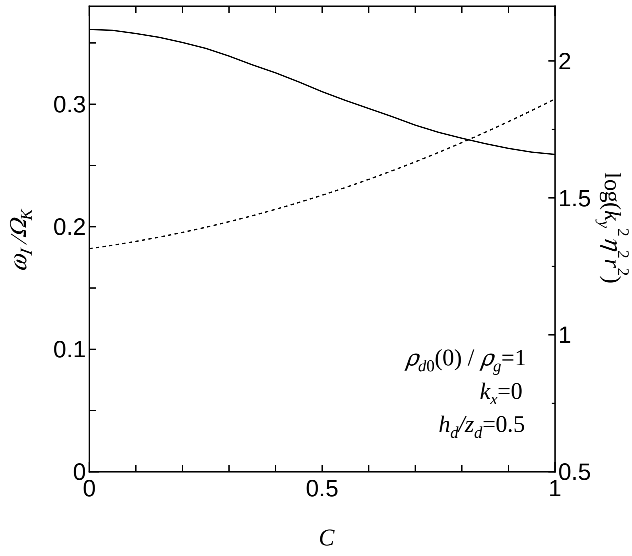

Fig. 1. The growth rate ω_I of the mode with the most unstable wave number as a function of the Coriolis parameter C in the case where $\rho_{d0}(0)/\rho_g = 1$ and $h_d/z_d = 0.5$ is shown by the solid curve. The most unstable mode has the radial wave number $k_x = 0$. The most unstable azimuthal wave number k_y squared which is normalized by η^2r^2 is shown by the dotted curve.

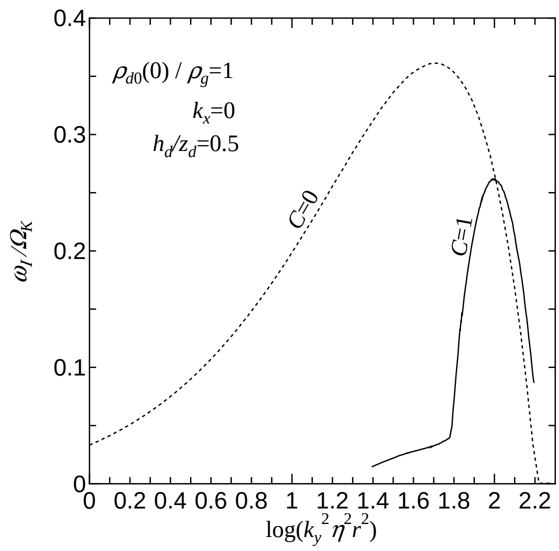

Fig. 2. The growth rate of instability ω_I as function of the azimuthal wave number squared for $C = 1$ (solid line) and $C = 0$ (dotted line), with $k_x = 0$, $\rho_{d0}(0)/\rho_g = 1$ and $h_d/z_d = 0.5$.

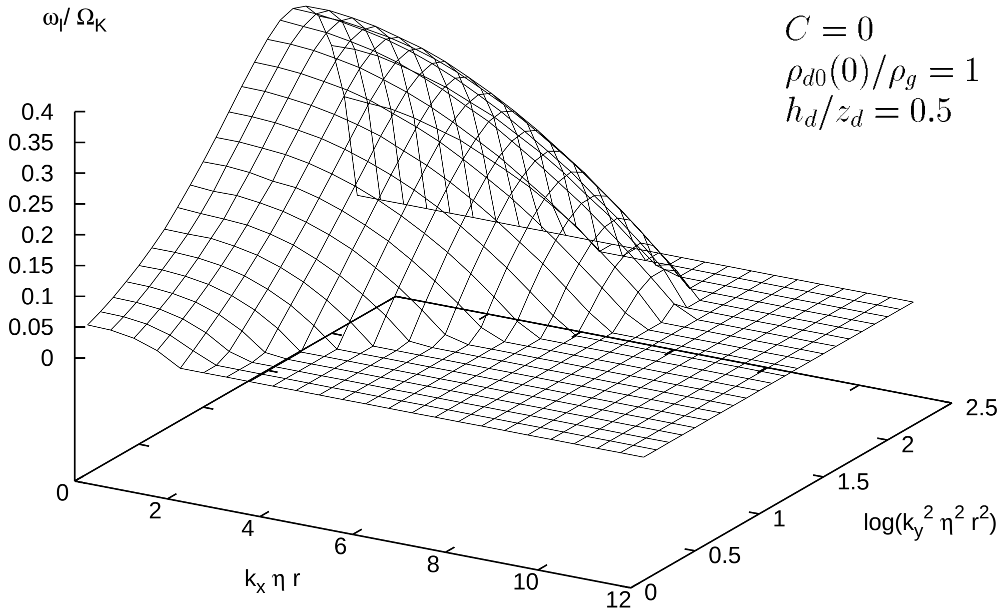

Fig. 3. The growth rate ω_I of the mode as a function of radial and azimuthal wave number k_x and k_y in the case where $C = 0$, $\rho_{d0}(0)/\rho_g = 1$ and $h_d/z_d = 0.5$.

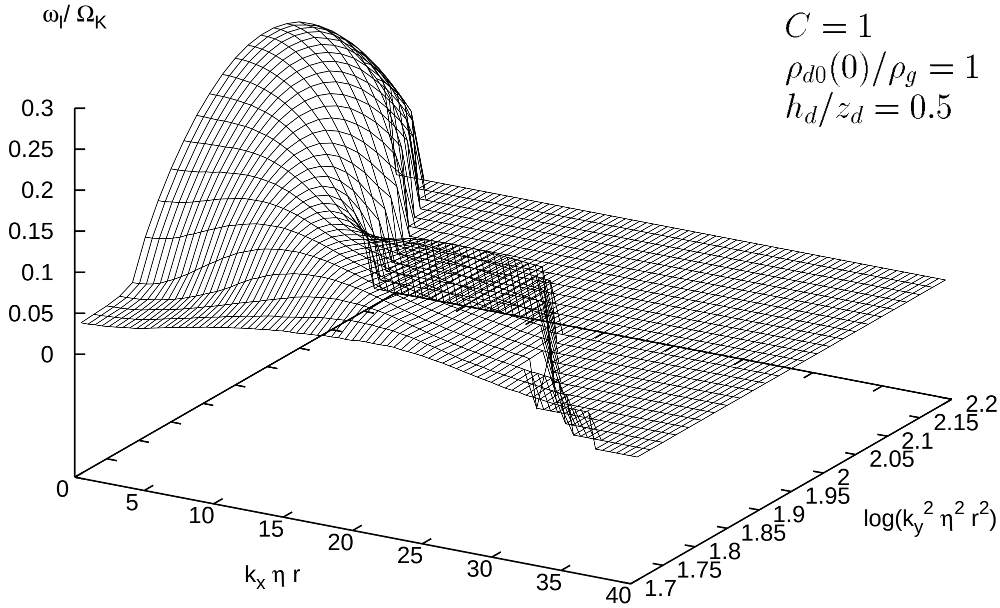

Fig. 4. Same as Fig. 3, but for $C = 1$.

Dotted and solid curves in Fig. 5 show the peak growth rates as functions of $\rho_{d0}(0)/\rho_g$ for $C = 0$ and 1, respectively. As dust settling proceeds, the difference in the growth rate by C decreases. In the case where the growth rate is much larger than Ω_K, the Coriolis force has little effect on the instability, as we have expected in Papers I and II.

It must be noted that neglecting the self-gravity of the fluid is invalid when its density approaches the critical density of the gravitational instability. The self-gravity would prevent the shear instability since it makes the Richardson number J increase. Here, we calculated the growth rates as functions of the wave number k_y at the critical density ($\rho_{d0}(0)/\rho_g = 260$) and $\rho_{d0}(0)/\rho_g = 100$ as references (Fig. 6). The growth rate is very large, and we expect that the tidal force, which is neglected in this paper, would have little effect in these cases.

Dotted and solid curves in Fig. 7 show the peak growth rates as functions of h_d/z_d for $C = 0$ and 1, respectively. When the transition zone of the dust layer h_d is very thin, the Coriolis force has little effect because the shear instability itself is so strong.

It turns out that in the case of the Coriolis force alone, the shear instability starts to grow before the dust density reaches the critical value of the gravitational instability by

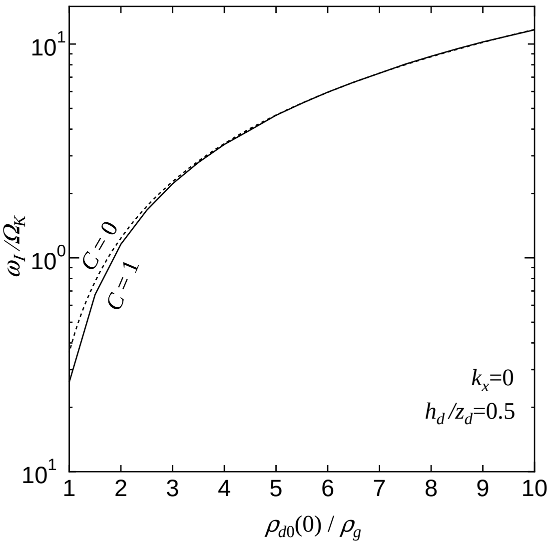

Fig. 5. The growth rate ω_I of the mode with the most unstable wave number as functions of the ratio of dust to gas on the midplane for $C = 1$ (solid curve) and $C = 0$ (dotted curve) in the case where $h_d/z_d = 0.5$.

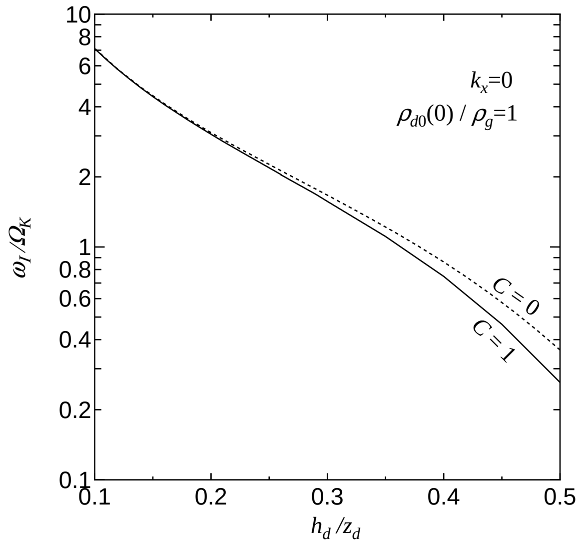

Fig. 7. The growth rate of instability ω_I as a function of h_d/z_d for $C = 1$(solid curve) and $C = 0$ (dotted curve) in the case where $\rho_{d0}(0)/\rho_g = 1$.

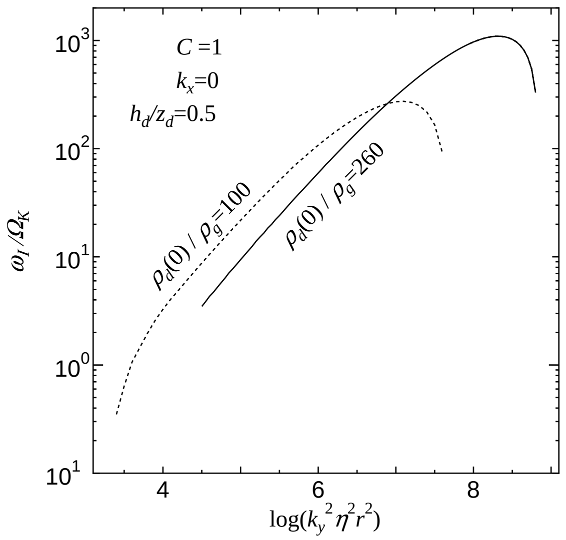

Fig. 6. The growth rate of instability ω_I as a function of the azimuthal wave number squared for the critical density ($\rho_{d0}(0)/\rho_g = 260$, solid curve) and $\rho_{d0}(0)/\rho_g = 100$ (dotted curve) in the case where $C = 1$ and $h_d/z_d = 0.5$.

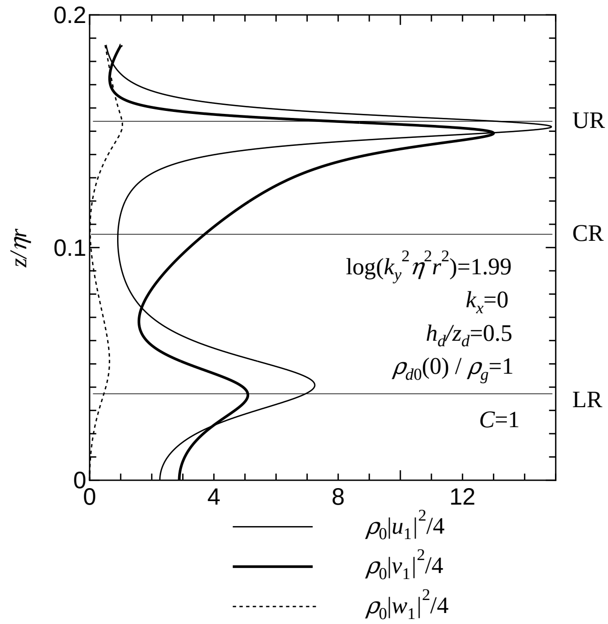

Fig. 8. The radial, azimuthal and vertical parts of the perturbed kinetic energy density, in the case for $C = 1$ where $\log(k_y^2\eta^2r^2) = 1.99$, with $k_x = 0$, $\rho_{d0}(0)/\rho_g = 1$ and $h_d/z_d = 0.5$. The horizontal line denoted by CR shows the co-rotation sheet. The horizontal lines denoted by UR and LR show the upper and lower resonances, respectively.

dust settling.

4. Discussion

The results in the previous section can be explained by means of energy equations. Multiplying Eq. (27) by $\rho_0 u_1^*/2$ and taking the real part, we have

$$2\omega_I \frac{1}{4}\rho_0|u_1|^2 = \frac{1}{2}k_x\Im(P_1u_1^*) + C\Omega_K v_0\Re(\rho_1 u_1^*) + C\Omega_K\rho_0\Re(v_1u_1^*). \tag{45}$$

This equation gives the radial part of the perturbed energy budget. Three terms on right-hand side denote powers due to perturbed pressure gradient, unperturbed pressure gradient (see Eq. (15)) and the Coriolis force. Multiplying Eq. (28) by $\rho_0 v_1^*/2$ and taking the real part, we have

$$2\omega_I \frac{1}{4}\rho_0|v_1|^2 = \frac{1}{2}k_y\Im(P_1v_1^*) - \frac{1}{2}\rho_0\frac{dv_0}{dz}\Re(w_1v_1^*) - C\Omega_K\rho_0\Re(u_1v_1^*). \tag{46}$$

This equation gives the azimuthal part of the perturbed energy budget. Three terms on right-hand side denote powers due to the perturbed pressure gradient, the unperturbed shear dv_0/dz and the Coriolis force. Multiplying Eq. (29)

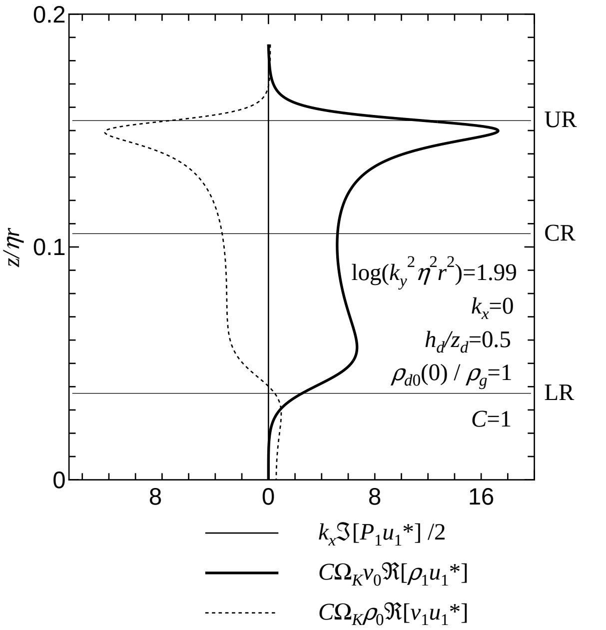

Fig. 9. Each term in the right hand side of the radial energy equation (Eq. (45)), in the case for $C = 1$ where $\log(k_y^2\eta^2 r^2) = 1.99$, with $k_x = 0$, $\rho_{d0}(0)/\rho_g = 1$ and $h_d/z_d = 0.5$.

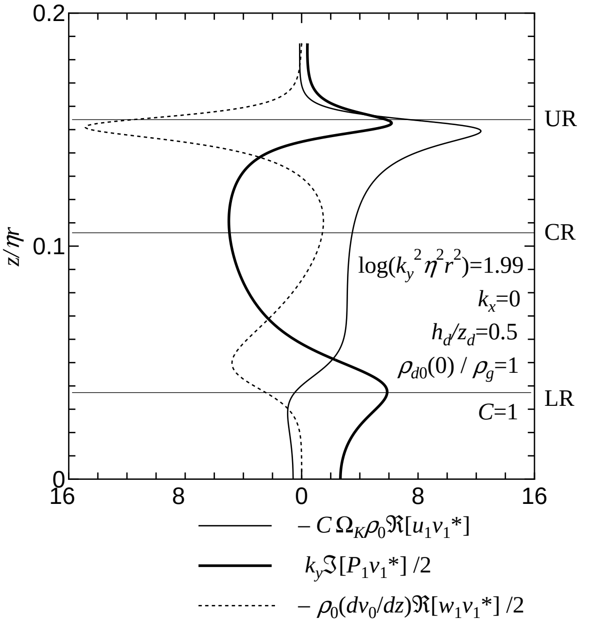

Fig. 10. Same as Fig. 9, but for azimuthal energy equation (Eq. (46)).

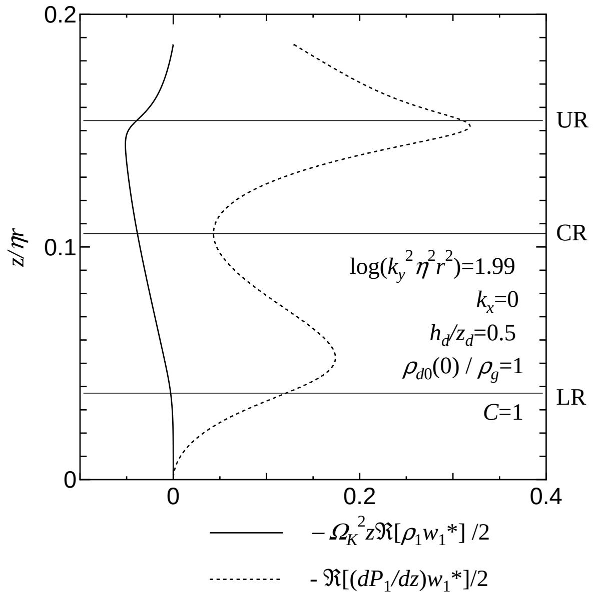

Fig. 11. Same as Fig. 9, but for the vertical energy equation (Eq. (47)).

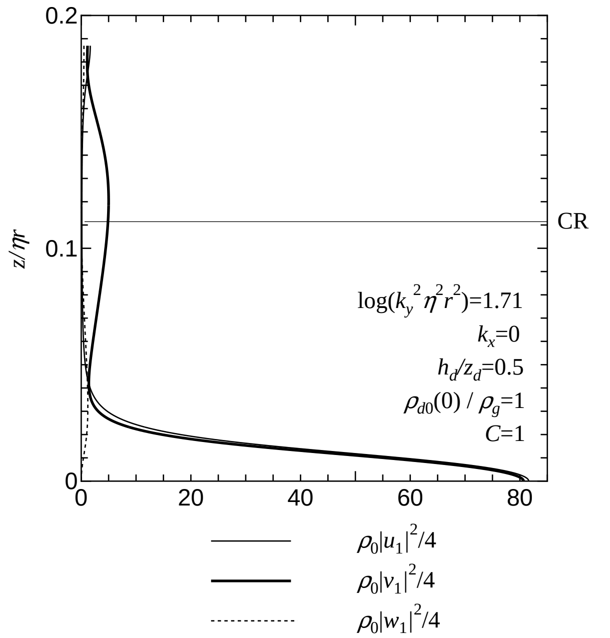

Fig. 12. Same as Fig. 8, but for $\log(k_y^2\eta^2 r^2) = 1.71$.

by $\rho_0 w_1^*/2$ and taking the real part, we have

$$2\omega_I \frac{1}{4}\rho_0|w_1|^2 = -\frac{1}{2}\Re(\frac{dP_1}{dz}w_1^*) - \frac{1}{2}\Omega_K^2 z\Re(\rho_1 w_1^*). \quad (47)$$

This equation gives the vertical part of the perturbed energy budget. Two terms on the right-hand side denote powers due to the perturbed pressure gradient and z-component of the gravity of the central star.

As described in Paper I, when $C = 0$, the azimuthal part of perturbed kinetic energy is supplied by the vertical shear dv_0/dz at the co-rotation sheet where $\bar{\omega} = 0$ and transported into the vertical part of perturbed kinetic energy through pressure. The vertical part of perturbed kinetic energy is lost by the work done by the z-component of the central star gravity $\Omega_K^2 z$. On the other hand, when $C = 1$, energy transport between radial and azimuthal directions occurs through the Coriolis force around new resonances (hereafter called merely "resonance"). These are resonances of a wave with the oscillation due to the Coriolis force. This resonance resembles the Lindblad resonance, which is the resonance with is the oscillation due to both the Coriolis and the tidal forces. The positions of resonances are given by

$$\Re(\bar{\omega}^2 - 4C^2\Omega_K^2) = 0. \quad (48)$$

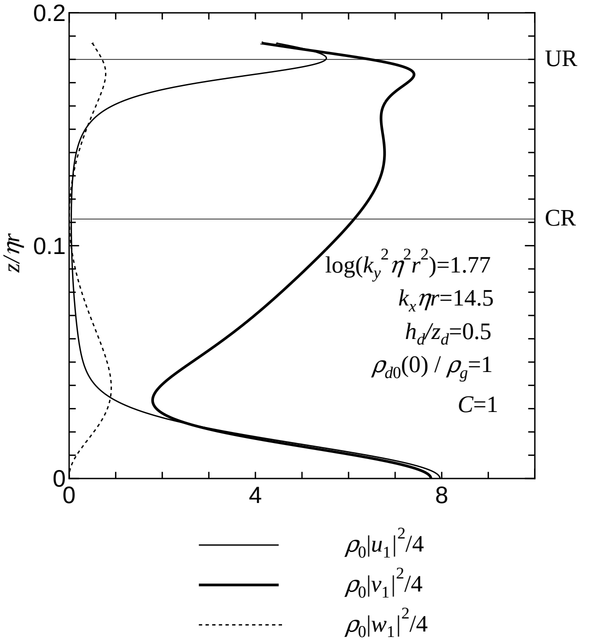

Fig. 13. Same as Fig. 8, but for $\log(k_y^2\eta^2r^2) = 1.77$ and $k_x\eta r = 14.5$.

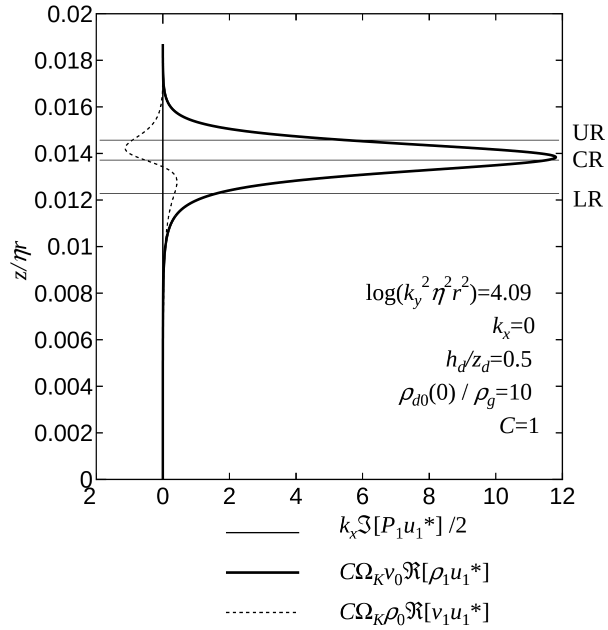

Fig. 15. Each term in the right hand side of the radial energy equation (Eq. (45)), in the case for $C = 1$ where $\log(k_y^2\eta^2r^2) = 4.09$, with $k_x = 0$, $\rho_{d0}(0)/\rho_g = 10$ and $h_d/z_d = 0.5$.

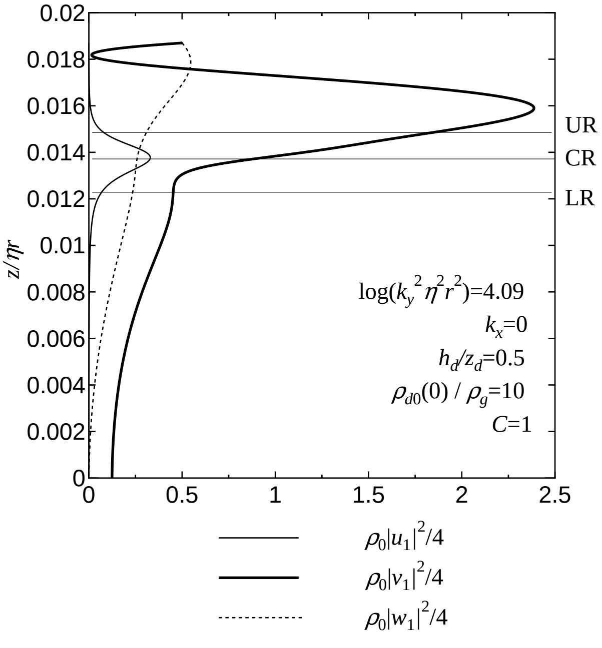

Fig. 14. Same as Fig. 8, but for $\rho_{d0}(0)/\rho_g = 10$ with $\log(k_y^2\eta^2r^2) = 4.09$ and $k_x = 0$.

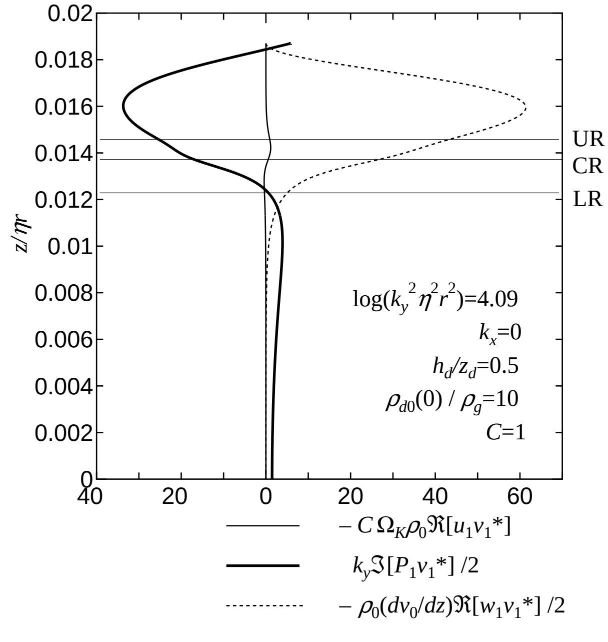

Fig. 16. Same as Fig. 15, but for the azimuthal energy equation (Eq. (46)).

At the resonance, a fluid element rotates around a guiding center. The latter orbit is circular (in our local analysis, a linear motion in y-direction). Figure 8 shows radial, azimuthal and vertical parts of the kinetic energy distribution for $C = 1$ at wave number $\log(k_y^2\eta^2r^2) = 1.99$, $k_x = 0$ where growth rate has the peak value for $\rho_{d0}(0)/\rho_g = 1$ and $h_d/z_d = 0.5$. Radial and azimuthal parts of energy concentrate around the upper resonance. The reason why the kinetic energy is small at the lower resonance compared to the upper one is probably due to the boundary conditions. Figures 9 to 11 show each term in the right hand sides of Eqs. (45) to (47) with the same parameters as Fig. 8, respectively. As for the x-direction, $C\Omega_K v_0\Re(\rho_1 u_1^*)$ is the term to gain energy from the unperturbed pressure gradient $\partial P_0/\partial x$ (see Eq. (15)). This is interpreted as a kind of the baroclinic instability (see e.g. Drazin and Reid, 1981). The term $C\Omega_K\rho_0\Re(v_1u_1^*)$ loses energy by converting radial to azimuthal parts of the kinetic energy through the Coriolis force. The term $k_x\Im(P_1u_1^*)/2$ is always zero because $k_x = 0$. As for the y-direction, the $-(dv_0/dz)\Re(w_1v_1^*)/2$ gets energy from the vertical shear when $C = 0$ (see figure 21 of Paper I). In the case $C = 1$

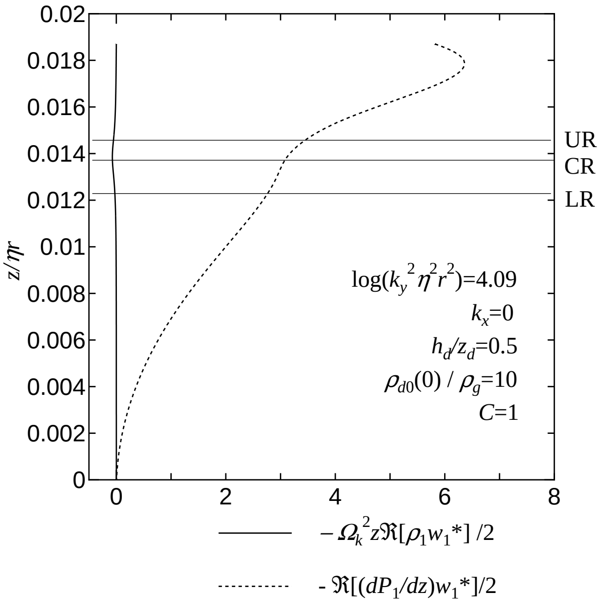

Fig. 17. Same as Fig. 15, but for the vertical energy equation (Eq. (47)).

with $\rho_{d0}(0)/\rho_g = 1$ and $h_d/z_d = 0.5$ (see Fig. 10), however, it rather loses energy except for the region around the co-rotation. As for the vertical part, almost same result as $C = 0$ holds except that the term $-\Re[(dP_1/dz)w_1^*]/2$ gains the energy at resonances in the case of $C = 1$ (see figure 21 of Paper I and Fig. 11). Thus, the Coriolis force plays role to suppress the shear instability but causes the baroclinic instability, so that the instability obtains more energy than we expected.

The slope of the curve of the growth rate becomes gentle for $\log(k_y^2\eta^2r^2) < 1.8$ (see Fig. 2). This is because both upper and lower resonances disappear in the density transition zone as seen in Fig. 8 with $\log(k_y^2\eta^2r^2) = 1.71$ in contrast to Fig. 11 with $\log(k_y^2\eta^2r^2) = 1.99$. Thus, the efficiency of transportation of energy from the radial part to azimuthal part decreases.

However, an upper resonance is present in the dust density transition zone for k_x larger than a finite value, even if $\log(k_y^2\eta^2r^2) \lesssim 1.8$ (Fig. 13). Thus, the growth rate has a peak at a certain value k_x for $\log(k_y^2\eta^2r^2) \lesssim 1.8$ (see Fig. 4).

Figure 14 shows the radial, azimuthal and vertical parts of the energy distribution for $\rho_{d0}(0)/\rho_g = 10$ and $h_d/z_d = 0.5$ with $\log(k_y^2\eta^2r^2) = 4.09$, $k_x = 0$ where the growth rate has the peak value. In the case $\rho_{d0}(0)/\rho_g = 10$, the perturbed kinetic energy gains more energy from the vertical shear than unperturbed pressure gradient dP_0/dz in contrast to the case $\rho_{d0}(0)/\rho_g = 1$ (see Figs. 15 to 17). Indeed, we find the radial part of the perturbed kinetic energy becomes small compared to the case where $\rho_{d0}(0)/\rho_g = 1$ (see Figs. 8 and 14). Thus, the larger $\rho_{d0}(0)/\rho_g$ is, the smaller the rotational effect is, as we have expected in Papers I and II.

5. Conclusions

In this paper, the linear stability analysis of the dust layer in the solar nebula is done including the effects of the Coriolis forces, but neglecting the effects of the tidal force. The following assumptions are adopted throughout this paper: (1) The self-gravity of the dust layer is neglected, since all the calculations are done with the dust densities below the critical density of the gravitational instability. (2) One fluid model is adopted, where the dust aggregates have the same velocity with the gas due to strong coupling by the drag force. This assumption is good for small compact dust aggregates (e.g. $\lesssim$1 cm at the terrestrial orbit) or for fluffy dust aggregates whose gas friction times are much smaller than the Kepler period, and the oscillation period and growth time of the instability. (3) The gas is incompressible, since the dust layer is very thin compared to the vertical scale height of the protoplanetary disk.

The calculated results with the Coriolis force but without the tidal force show that the dust layer is not stabilized by the Coriolis force only. The growth rates of the instabilities are similar in the cases with and without the Coriolis force.

The energy source of the instability is investigated. In contrast to the case without the Coriolis force where the energy is supplied from around the co-rotation point, the calculations with the Coriolis force show that the energy is supplied from around the resonance of a wave and the epicyclic motion with the oscillation due to the Coriolis force for $\rho_d(0)/\rho_g \lesssim 1$, where the growth rate of the instability $\omega_I \lesssim \Omega_K$. For $\rho_d(0)/\rho_g \gtrsim 10$, on the other hand, the energy source of the instability is the vertical shear as in the model without the Coriolis force.

Our subsequent paper will show calculations with not only the Coriolis force but also the tidal force of the central star.

Acknowledgments. We thank Drs. Yoshitsugu Nakagawa, Stuart J. Weidenschilling, Sei-Ichiro Watanabe, Saburo Miyahara and Shin-Ichi Takehiro for valuable comments. Numerical calculations were performed partly at the Astronomical Data Analysis Center of the National Astronomical Observatory, Japan.

References

Adachi, I., C. Hayashi, and K. Nakazawa, The gas drag effect on the elliptical motion of a solid body in the primordial solar nebula, *Prog. Theor. Phys.*, **56**, 1756–1771, 1976.

Champney, J. M., A. R. Dobrovolskis, and J. N. Cuzzi, A numerical turbulence model for multiphase flows in the protoplanetary nebula, *Phys. Fluids*, **7**, 1703–1711, 1995.

Coradini, A., C. Frederico, and G. Magni, Formation of planetesimals in an evolving protoplanetary disk, *Astron. Astrophys.*, **98**, 173–185, 1981.

Cuzzi, J. N., A. R. Doborvolskis, and J. M. Champney, Particle-gas dynamics in the midplane of a protoplanetary nebula, *Icarus*, **106**, 102–134, 1993.

Dobrovolskis, A. R., J. S. Dacles-Mariani, and J. N. Cuzzi, Production and damping of turbulence by particles in the solar nebula, *J. Geophys. Res.*, **104**(E21), 30805–30815, 1999.

Drazin, P. G. and W. H. Reid, *Hydrodynamic Stability*, Cambridge Univ. Press, 1981.

Goldreich, P. and W. R. Ward, The formation of planetesimals, *Astrophys. J.*, **183**, 1051–1061, 1973.

Hayashi, C., Structure of the solar nebula, growth and decay of magnetic fields and effects of magnetic and turbulent viscosities on the nebula, *Progr. Theor. Phys. Suppl.*, **70**, 35–53, 1981.

Hayashi, C., K. Nakazawa, and Y. Nakagawa, Formation of the solar system, in *Protostars and Planets II*, edited by B. C. Black and M. S. Matthews, pp. 1100–1153, Univ. of Arizona Press, Tucson, 1985.

Nakagawa, Y., K. Nakazawa, and C. Hayashi, Growth and sedimentation of dust grains in the primordial solar nebula, *Icarus*, **45**, 517–528, 1981.

Nakagawa, Y., M. Sekiya, and C. Hayashi, Settling and growth of dust particles in a laminar phase of a low-mass solar nebula. *Icarus*, **67**, 375–390, 1986.

Safronov, V. S., *Evolution of the Protoplanetary Cloud and Formation of the Earth and the Planets*, Nauka, Moscow, [*NASA Tech. Trans. F-677*],

1969.
Sekiya, M., Gravitational instability in a dust-gas layer and formation of planetesimals in the solar nebula, *Progr. Theor. Phys.*, **69**, 1116–1130, 1983.
Sekiya, M., Quasi-equilibrium density distributions of small dust aggregations in the solar nebula, *Icarus*, **133**, 298–303, 1998.
Sekiya, M. and N. Ishitsu, Shear instabilities in the dust layer of the solar nebula I. The linear analysis of a non-gravitating one-fluid model without the Coriolis and the solar tidal forces, *Earth Planets Space*, **52**, 517–526, 2000.
Sekiya, M. and N. Ishitsu, Shear instabilities in the dust layer of the solar nebula II. Different unperturbed states, *Earth Planets Space*, **53**, 761–765, 2001.
Shu, F. H., *The Physics of Astrophysics II. Gas Dynamics*, University Science Books, 1992.
Watanabe, S. and T. Yamada, Numerical simulations of dust-gas 2-phase flows in the solar nebula, *Eos, Trans. Am. Geoph. Union Suppl.*, **81**, No. 22, WP99, 2000.
Weidenschilling, S. J., Dust to planetesimals: settling and coagulation in the solar nebula, *Icarus*, **44**, 172–189, 1980.
Weidenschilling, S. J., Evolution of grains in a turbulent solar nebula, *Icarus*, **60**, 553–567, 1984.
Weidenschilling, S. J. and J. N. Cuzzi, Formation of planetesimals in the solar nebula, in *Protostars and Planets III*, edited by E. H. Levy and J. I. Lunine, pp. 1031–1060, Univ. of Arizona Press, Tucson, 1993.

N. Ishitsu (e-mail: ishitsu@qdeps.geo.kyushu-u.ac.jp) and M. Sekiya